CrossMark

RESEARCH ARTICLE

Arsenic sorption by red mud-modified biochar produced from rice straw

Chuan Wu[1] · Liu Huang[1] · Sheng-Guo Xue[1] · Yu-Ying Huang[2] · William Hartley[3] ·
Meng-qian Cui[1] · Ming-Hung Wong[4]

Abstract Red mud-modified biochar (RM-BC) has been produced to be utilized as a novel adsorbent to remove As because it can effectively combine the beneficial features of red mud (rich metal oxide composition and porous structure) and biochar (large surface area and porous structure properties). SEM-EDS and XRD analyses demonstrated that red mud had loaded successfully on the surface of biochar. With the increasing of pH in solution, arsenate (As(V)) adsorption on RM-BC decreased while arsenite (As(III)) increased. Arsenate adsorption kinetics process on RM-BC fitted the pseudo-second-order model, while that of As(III) favored the Elovich model. All sorption isotherms produced superior fits with the Langmuir model. RM-BC exhibited improved As removal capabilities, with a maximum adsorption capacity (Q_{max}) for As(V) of 5923 $\mu g\ g^{-1}$, approximately ten times greater than that of the untreated BC (552.0 $\mu g\ g^{-1}$). Furthermore, it has been indicated that the adsorption of As(V) on RM-BC may be strongly associated with iron oxides (hematite and magnetite) and aluminum oxides (gibbsite) by X-ray absorption near-edge spectroscopy (XANES), which was possibly because of surface complexation and electrostatic interactions. RM-BC may be used as a valuable adsorbent for removing As in the environment due to the waste materials being relatively abundant.

Keywords Red mud · Biochar · Arsenate · Hematite · Magnetite · Gibbsite

Responsible editor: Guilherme L. Dotto

✉ Sheng-Guo Xue
    sgxue@csu.edu.cn

[1] School of Metallurgy and Environment, Central South University, Changsha 410083, People's Republic of China

[2] Shanghai Synchrotron Radiation Facility (SSRF), Shanghai Institute of Applied Physics, Chinese Academy of Sciences, Shanghai 201204, People's Republic of China

[3] Crop and Environment Sciences Department, Harper Adams University, Newport, Shropshire TF10 8NB, UK

[4] Consortium on Health, Environment, Education and Research (CHEER), The Education University of Hong Kong, Tai Po, Hong Kong Special Administrative Region, People's Republic of China

Introduction

Arsenic (As) as a metalloid has been considered to be a proverbial carcinogen. Many anthropogenic activities including the use of insecticides, phosphate fertilizers, mining, and smelting operations have released As into soils and groundwater and thus caused global environment contamination (Kim et al. 2014; Xue et al. 2017). Arsenic-contaminated soils are harmful to food safety and groundwater quality, and eventually threaten human health in many regions of the world such as Mexico, USA, China, Bangladesh, and Pakistan (Jadhav et al. 2015). As compounds exist either as inorganic and organic species (Wu et al. 2016a). Generally, compared with organic As forms, inorganic As species are more detrimental to organisms (Wu et al. 2016b; Wu et al. 2017). Therefore, it is urgent to control the entrance of As especially inorganic As into natural environment. In order to solve the problem of As pollution, many studies are focusing on developing various kinds of adsorbed materials.

Red mud (RM), known as the popular name of bauxite residue, is the residue generated from the process of Al production by Bayer (Xue et al. 2016a; Zhu et al. 2016a). Due to the difficulty of disposal and large volumes (120 million tons per year), it is essential to find alternative options for red mud treatment and use (Xue et al. 2016b; Kong et al. 2017a).

Generally, the mineralogical composition of red mud consists of diversified forms of iron and aluminum oxides, calcium and sodium aluminum silicates. Red mud has a fine, porous structural nature and its surface carries significant hydroxyl groups (Liu and Naidu 2014; Zhu et al. 2017). As a result, the material has great potential to remediate As contamination both in soils and groundwater. Previous studies confirmed that red mud, or neutralized red mud by different methods, has the ability to mitigate As in aquatic environment (Altundogan et al. 2000; Guo et al. 2014). Furthermore, it has been demonstrated that RM can inhibit the uptake of As by crops for it will transform from unstable As fractionation to stable forms in soils (Yan et al. 2013; Hua et al. 2017). The interaction mechanisms between As and red mud can be mainly attributed to electrostatic attraction/repulsion, chemical interaction (Castaldi et al. 2010).

Biochar is a stable solid derived from rich carbonaceous biomass which processing thermal or hydrothermal transformation under oxygen-limiting circumstances (Zhang et al. 2013). It has been used in numerous applications mostly as a soil amendment/conditioner, a waste management tool and to mitigate global warming (Khan et al. 2013). Furthermore, biochar is able to enhance soil luxuriance, elevate the bioavailability of soil nutrient, enhance agricultural productivity, and sequester carbon (Lone et al. 2015). However, there is evidence that biochar may also inhibit the bioavailability of essential plant micronutrients (Hartley et al. 2016). Additionally, biochar can effectively remove water contaminants (such as As, Cr and Cd) because of its favorable physicochemical properties (large surface area and porous structure and contains oxygen functional groups and aromatic compounds on its surface) (Tan et al. 2016). The properties of biochar, mainly the large surface area and cation exchange capacity (CEC), can stabilize several kinds of heavy metals like Pb, Zn, Cu (Lu et al. 2017).

Conversely, it has been demonstrated that biochar can elevate soil pH and thus mobilize As, which has limited its application in As remediation (Wang et al. 2017). Recently, investigations have been focusing on the application of biochar-based materials that have enhanced capabilities as adsorbents for removing As from water and soils. Biochar-based materials including $ZnCl_2$-activated biochar, and Ca-/Fe-modified biochar have been applied to mitigate As from water (Samsuri et al. 2013; Xia et al. 2016). In spite of these good effects, biochar-based materials are comparatively complex and expensive to prepare.

Biochar has a porous structure that can be used to support the distribution of particles within its matrix (Wang et al. 2015c). Red mud shows some potential for As adsorption due to its distinctive oxide-rich constitution, especially iron and aluminum oxides, surface hydroxyl groups and its porous nature (Wang et al. 2008; Zhu et al. 2016b, c). Both rice straw and red mud are low-cost, abundant materials. Such is rarely concerned that composite materials composed of red mud and biochar seem to be effective to As remediation. Based on premises, the study attempts to develop a novel red mud-modified biochar, in order to (1) characterize its physicochemical properties, (2) compare the kinetics of As sorption by red mud-modified biochar and untreated biochar produced from rice straw, and (3) investigate adsorption mechanisms using X-ray absorption spectroscopy (XANES).

Materials and methods

Experiment materials

In the present experiment, sodium arsenite ($NaAsO_2$) and sodium arsenate ($Na_2HAsO_4 \cdot 12H_2O$) were purchased from Aldrich Chemical Co. Rice straw was collected from a rice field located around the downtown of Wangcheng (Changsha city of Hunan, P.R. China). It was air-dried, milled into powder (0.15 mm), and then used for biochar production (Lu et al. 2017). Red mud (RM), obtained from the Guangxi Pingguo alumina refinery (Pingguo, Guangxi Province, China), was oven-dried overnight at 60 °C.

Biochar preparation

Red mud-modified biochar (RM-BC) was produced using the method adopted by Yao et al. (2014). The mixture solution was prepared by 2 g of raw RM and 500 mL deionized water and then stirred for 30 min to obtain stable RM suspensions. Subsequently, 10 g of rice straw was thoroughly mixed with the RM suspension and the mixture was stirred for 2 h. Finally, the RM-modified feedstock was obtained by filtering and then oven-drying at 80 °C.

Pyrolysis of the RM-modified feedstock took place in a muffle furnace (SX$_2$-5-12, Yuandong Therm corporaion in Changsha, China) at 600 °C. In order to maintain biomass pyrolysis process preparation conditions, oxygen-free N_2 was circulated into the system at a flowrate of 200 mL/min. The temperature increased at a rate of 5 °C/min until 600 °C. The raw materials were pyrolyzed in a muffle furnace for 6 h. After cooling to room temperature (25 °C), prepared materials were washed by deionized water for three times with the purpose of eliminating foreign substances, and oven dried at 80 °C. Rice straw without RM modification was prepared by the same process. Hereafter, red mud-modified biochar and untreated biochar are named RM-BC and BC, respectively.

Material characterization

BC and RM-BC were dried and sieved for instrument analysis. The surface areas were measured via surface area analyzer and calculated by the method of N_2-BET. Variant morphologies and

elements analysis of the BC and RM-BC were recorded by scanning electron microscope which equipped with energy-dispersive X-ray spectroscopy (SEM-EDS, Phenom XL). Furthermore, the crystal structure of these biochar-based materials was detected through X-ray powder diffraction (XRD).

The effects of solution pH on adsorption

10 mg/L As(V) and 10 mg/L As(III) as working solutions were obtained through diluting stock solutions prepared by dissolving $Na_2HAsO_4·12H_2O$ and $NaAsO_2$ respectively. The working solutions contained 0.01 mol/L NaCl can be capable to keep a stable ionic strength. Approximately 0.12 g of BC or RM-BC was added to 30 mL As(V)/As(III) working solutions of the different pH values to make 4 g L^{-1} concentrations. Then, the solution pH was adjusted to 2, 4, 6, 8, 10, and 12, respectively, using 0.1 mol L^{-1} HCl/NaOH (Feng et al. 2015). Subsequently, these samples were shaken at a constant temperature (25 ± 1 °C) in an oscillator bath (DDHZ-300, Experimental facility corporation in TaiCang) at 200 rpm/min for 24 h. Samples were then immediately passed through syringe membrane filters (0.45 μm) to determine As concentrations. Total As in the filtrate was measured by the instrument of HG-AFS. Each treatment had three repetitions. The As adsorbed concentration q (μg g^{-1}) was calculated as follows:

$$q = \frac{(C_0 - C_t)V}{m} \quad (1)$$

where q (μg g^{-1}) means As adsorbed concentration at equilibrium; C_0 and C_t (μg L^{-1}) refer to the original and equilibrium solute concentrations individually; V (L) on behalf of solute volume and m (g) indicates the adsorbents amount.

Adsorption kinetics

To investigate As adsorption mechanisms, adsorption kinetic studies were implemented at around 25 °C. Approximately 0.12 g (4 g L^{-1}) of BC and RM-BC were added to 30 mL 10 mg L^{-1} As(V) solutions; the pH of these mixture were respectively adjusted to 6 and 2 based on the former study. In addition, 0.12 g (4 g L^{-1}) of BC and RM-BC also were added to 30 mL 10 mg L^{-1} As(III) solutions. The pH of the mixture was regulated to 10 employing HCl or NaOH. All the treatments were then shaken at 200 rpm/min for predetermined different time periods of 0.5, 1, 2, 4, 8, 12, 16, and 24 h, respectively. The pH of all mixture solution changed lower than 0.5~0.8 unit. Samples were filtered for As determination via HG-AFS. Each treatment had three repetitions.

Kinetics data were fitted with four classical kinetics models to reveal the adsorption mechanism. The governing equations of the mathematical models are listed as follows:

$$pseudo-first-order: \quad \frac{dqt}{dt} = k1(qe-qt) \quad (2)$$

$$pseudo-second-order: \quad \frac{dqt}{dt} = k2(qe-qt)^2 \quad (3)$$

$$Elovich: \quad \frac{dqt}{dt} = \alpha \exp(-\beta qt) \quad (4)$$

$$intraparticle\ diffusion: \quad q_t = K_d t^{\frac{1}{2}} + C \quad (5)$$

where q_t and q_e (μg/g) represent the adsorbent remove As concentrations at t time and equilibrium time, and k_1 (h^{-1}), k_2 (g μg^{-1} h^{-1}), and k_d (μg g^{-1} min$^{-1/2}$) are the rate of kinetic constants; C (μg g^{-1}) is the y-intercept. Initial adsorption rate is regarded as α (μg g^{-1}) and β (μg g^{-1}) the desorption constant.

Adsorption isotherms

Adsorption equilibrium isotherms for As adsorption on RM-BC and BC were measured at various As level (1–50 mg/L As(V)/As(III)). Equilibrium adsorption investigations were performed for 24 h. The change of the solution pHs was small. Each treatment had three repetitions. The models of Langmuir and Freundlich were used to explain adsorption isotherms. Equations were as listed below:

$$Langmuir: \quad q_e = \frac{q_m k_L C_e}{1 + K_L C_e} \quad (6)$$

$$Freundlich: \quad q_e = K_F C_e^{\ n} \quad (7)$$

where q_e (μg g^{-1}) indicates the adsorbed As concentration at equilibrium; C_e (mg L^{-1}) represents the equilibrium concentration of As; q_m (μg g^{-1}) denotes the maximum adsorption capacity and n refers parameter; K_L (L mg^{-1}) and K_F represent the constants of Langmuir and Freundlich, respectively.

R_L (the equilibrium parameter in the Langmuir model) used to be employed to determine whether adsorption is favorable or not, is as follows (Sun et al. 2015):

$$R_L = \frac{1}{1 + K_L C_0} \quad (8)$$

where C_0 (mg L^{-1}) suggests the incipient concentration of As and K_L (L mg^{-1}) represents Langmuir constant.

XANES analysis

Mechanism of As(V) sorption on RM-BC was detected by X-ray absorption spectroscopy (XANES). All minerals (hematite, magnetite, goethite, and gibbsite) were obtained from Sigma primarily aimed at reference spectra. Approximately 4 g L^{-1} of each mineral was applied to 30 mL of As(V) solution (10 mg· L^{-1}) for 24 h using 0.01 mol·L^{-1} NaCl to maintain ionic strength. The suspension was centrifuged and then filtered.

Solid samples were washed with ultrapure water, and then freeze-dried for subsequent analysis. The data were acquired at beamline BL14W at the Shanghai Synchrotron Radiation Facility (SSRF). Data was processed by Athena IFEFFIT package and SixPack to quantitatively determine As species.

Data analysis

The data in the paper was processed by Microsoft Excel 2010 and SPSS 19.0 and photographs were fabricated by Origin 9.0.

Fig. 1 SEM-EDS of biochar (BC) and red mud-modified biochar (RM-BC). a BC, b RM-BC before adsorption, c RM-BC after adsorption of As(V), d RM-BC after adsorption of As(III)
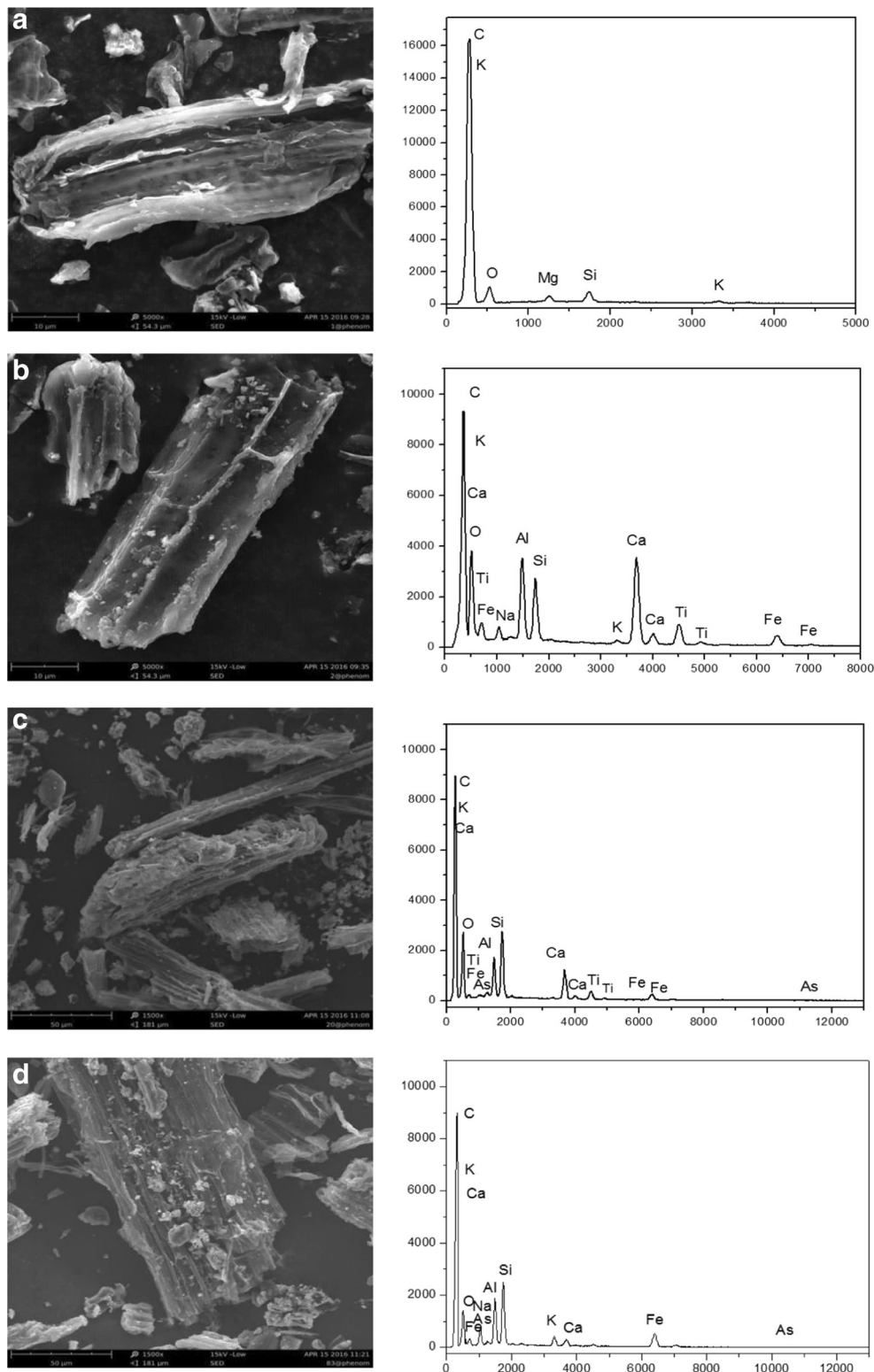
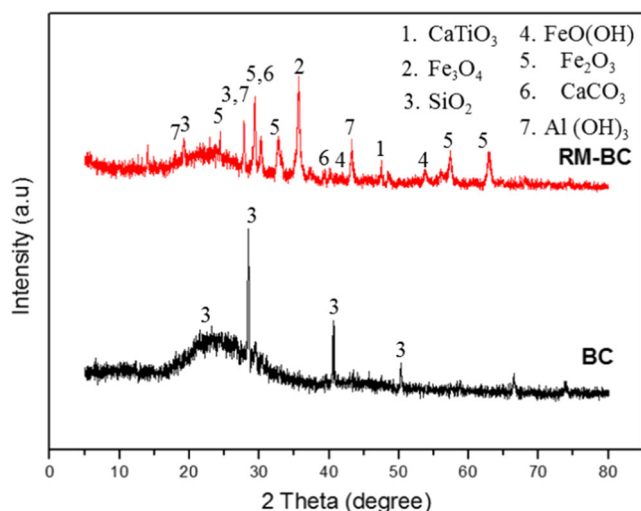**Fig. 2** XRD spectra of biochar (BC) and red mud-modified biochar (RM-BC)

Results and discussion

BC and RM-BC characterization

The BET N_2 surface areas of BC and RM-BC were 210.29 and 186.95 m^2/g. The morphology images and EDX of RM and RM-BC are shown in Fig. 1. The EDX spectrum and SEM confirmed that the surface of biochar was loaded with red mud. The EDX analysis of RM-BC revealed extra peaks for calcium, iron, aluminum, titanium and sodium, which are the elemental compositions of red mud when compared to that of BC (Fig. 1b). The surface of RM-BC appeared smooth without adsorption (Fig. 1b) and then became coarser after As(V) adsorption process (Fig. 1c) and As(III) removal process (Fig. 1d). The EDS spectra analysis showed that As was coated on the surface of the RM-BC, demonstrating that adsorption had occurred (Fig. 1c, d).

The structures of RM-BC and BC were clearly different, when detected by XRD. The crystalline phases of RM-BC were probed and identified as hematite, magnetite, goethite,

calcite, gibbsite, and perovskite which were not detected in the crystalline phases of BC (Fig. 2). The results further confirmed that red mud had been successfully loaded on the surfaces of the biochar matrix.

The effect of solution pH

Figure 3a, b respectively showed the effect of different pH on the As adsorption process of each biochar (BC/RM-BC). The quantity of adsorbed As(V) (q, $\mu g\ g^{-1}$) decreased with increasing pH on RM-BC (Fig. 3a). The maximum adsorption density for As(V) at pH = 2 was 1622.51 $\mu g\ g^{-1}$. Adsorption capacity of BC for As(V) raised in the wake of pH from 2 to 6, but then reduced when the pH ranged from 6 to 12. The maximum adsorption of BC was q = 481.61 $\mu g\ g^{-1}$ at pH = 6. Biochar had a somewhat lower As(V) removal capacity, contrasted with that of RM-BC.

The influence of pH on As(III) adsorption are presented in Fig. 3b. Clearly, BC and RM-BC showed similar trends on the pH-dependent adsorption curves. The quantity adsorbed As(III) was on the rise following the solution pH from 2 to 10, but when pH was elevated from 10 to 12, the adsorbed amount for As(III) of both BC and RM-BC reduced. Overall, the results indicated that As(V) is adsorbed in acidic pH conditions, but As(III) tends to be adsorbed in alkaline pH circumstances. In addition, red mud modification significantly enhanced the sorption ability of biochar both on As(V) and As(III).

pH is considered as a crucial factor influencing As species distribution and the surface charge of BC/RM-BC. Anionic species of arseneous and arsenic acids are dictated by pH. Ionization equations are as listed below:
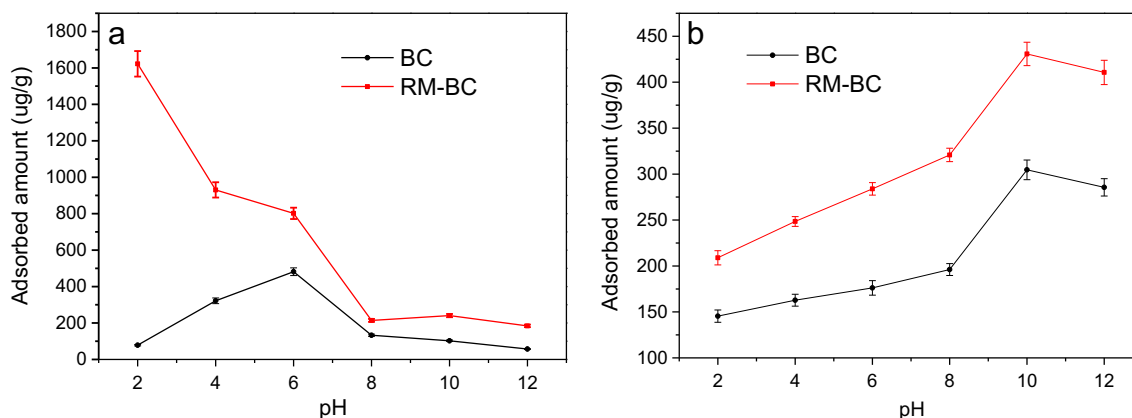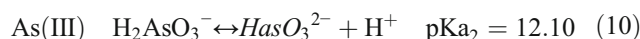
$$H_3AsO_3 \leftrightarrow H_2AsO_3^- + H^+ \quad pKa_1 = 9.23 \tag{9}$$

$$As(III) \quad H_2AsO_3^- \leftrightarrow HasO_3^{2-} + H^+ \quad pKa_2 = 12.10 \tag{10}$$

$$HasO_3^{2-} \leftrightarrow AsO_3^{3-} + H^+ \quad pKa_3 = 13.41 \tag{11}$$

Fig. 3 Effects of pH on the concentration of **a** As(V) and **b** As(III) adsorbed by BC and RM-BC
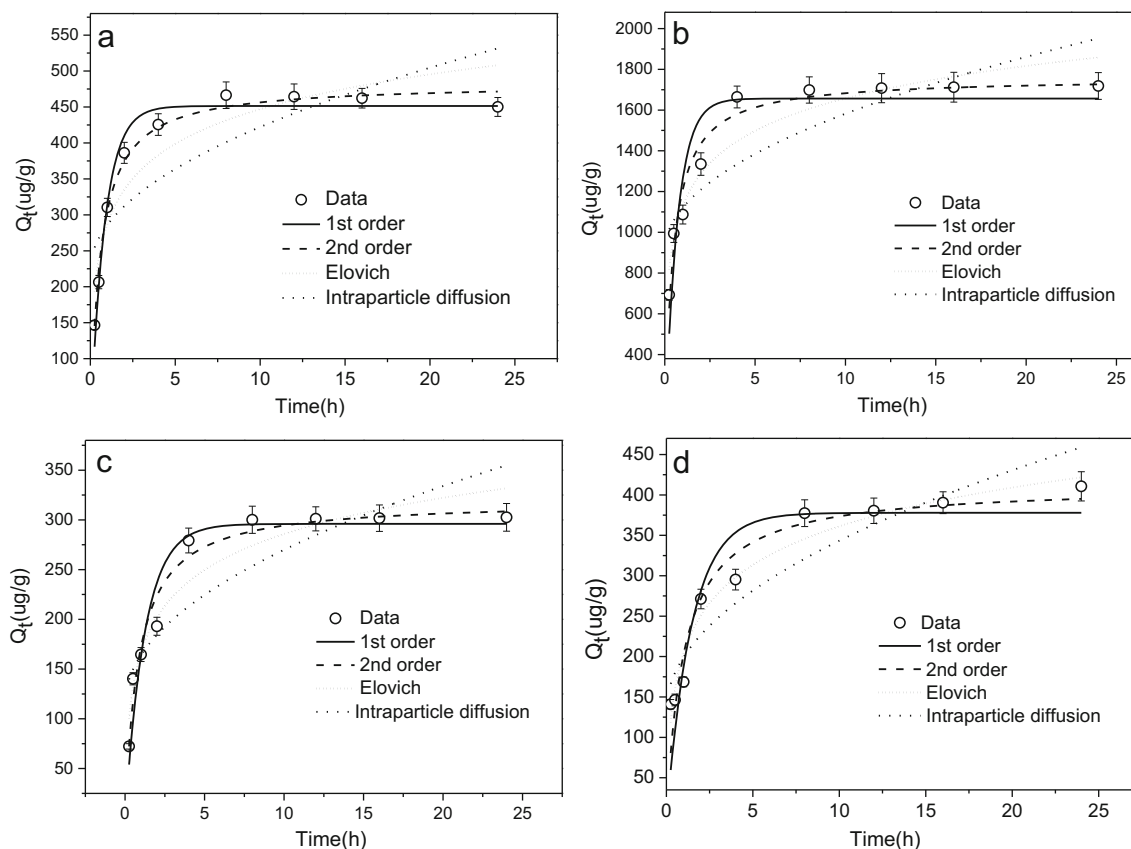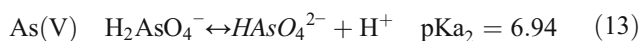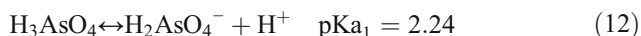
Fig. 4 Adsorption kinetics and modeling for As on adsorbents: **a** and **b** are As(V) adsorption on BC and RM-BC, respectively. **c** and **d** are As(III) adsorption on BC and RM-BC, respectively

$$H_3AsO_4 \leftrightarrow H_2AsO_4^- + H^+ \quad pKa_1 = 2.24 \quad (12)$$

$$As(V) \quad H_2AsO_4^- \leftrightarrow HAsO_4^{2-} + H^+ \quad pKa_2 = 6.94 \quad (13)$$

$$HAsO_4^{2-} \leftrightarrow AsO_4^{3-} + H^+ \quad pKa_3 = 11.50 \quad (14)$$

Given pH < pH$_{PZC}$ (point of zero charge), positive charges will form on the surface of biochar. At this time, As(V) predominantly as H$_2$AsO$_4^-$ form and adsorption occurs by electrostatic and chemical attraction (Cheng et al. 2016). At higher pH values, the major As species exist as HAsO$_4^{2-}$ and AsO$_4^{3-}$. However, the availability of binding sites declines with increasing pH. When the pH is above the pH$_{PZC}$ adsorbent surfaces develop negative charges, which repulse anions including HAsO$_4^{2-}$ and AsO$_4^{3-}$. In the meantime, OH$^-$ will

compete with As anion for positively charged surface sites, and as a result weaken the adsorption process (Feng et al. 2015). However, the pHpzc value of red mud could not be accurately determined since some components of red mud were solubilized during the potentiometric titration (Altundogan et al. 2000). Furthermore, some studies reported that the properties and mineralogical composition of RM will be changed by pH and specific sorption locations of RM will decrease with increasing pH (Castaldi et al. 2010; Kong et al. 2017b).

The adsorbed volume of As(III) reached its maximum between pH 8 and 10 (Fig. 3b). This is agreed with the consequence of Manju et al. (1998) which used copper impregnated activated carbon as a sorbent, and discovered that As(III)

Table 1 Kinetic models and best-fit parameters for As adsorption data

| sample		First-order			Second-order			Elovich			Intraparticle diffusion		
		$k_1(h^{-1})$	$q_e(\mu g/g)$	R^2	$k_2(g\ \mu g^{-1}\ h^{-1})$	$q_e(\mu g/g)$	R^2	$\beta(\mu g/g)$	$\alpha(\mu g/g)$	R^2	$K_d(\mu g\ g^{-1}\ min^{-1/2})$	$C(\mu g/g)$	R^2
BC	As(V)	1.195	451.4	0.983	0.00357	482.9	0.987	0.0143	4168.5	0.884	62.96	233.1	0.6664
RM-BC	As(V)	1.446	1656.5	0.900	0.00126	1758.6	0.957	0.00435	31,085.8	0.917	212.94	908.7	0.7298
BC	As(III)	0.805	296.0	0.948	0.00366	319.5	0.960	0.0190	1196.7	0.928	48.95	115.1	0.7662
RM-BC	As(III)	0.686	377.9	0.911	0.00236	412.0	0.927	0.0144	1253.1	0.962	66.57	132.9	0.8842
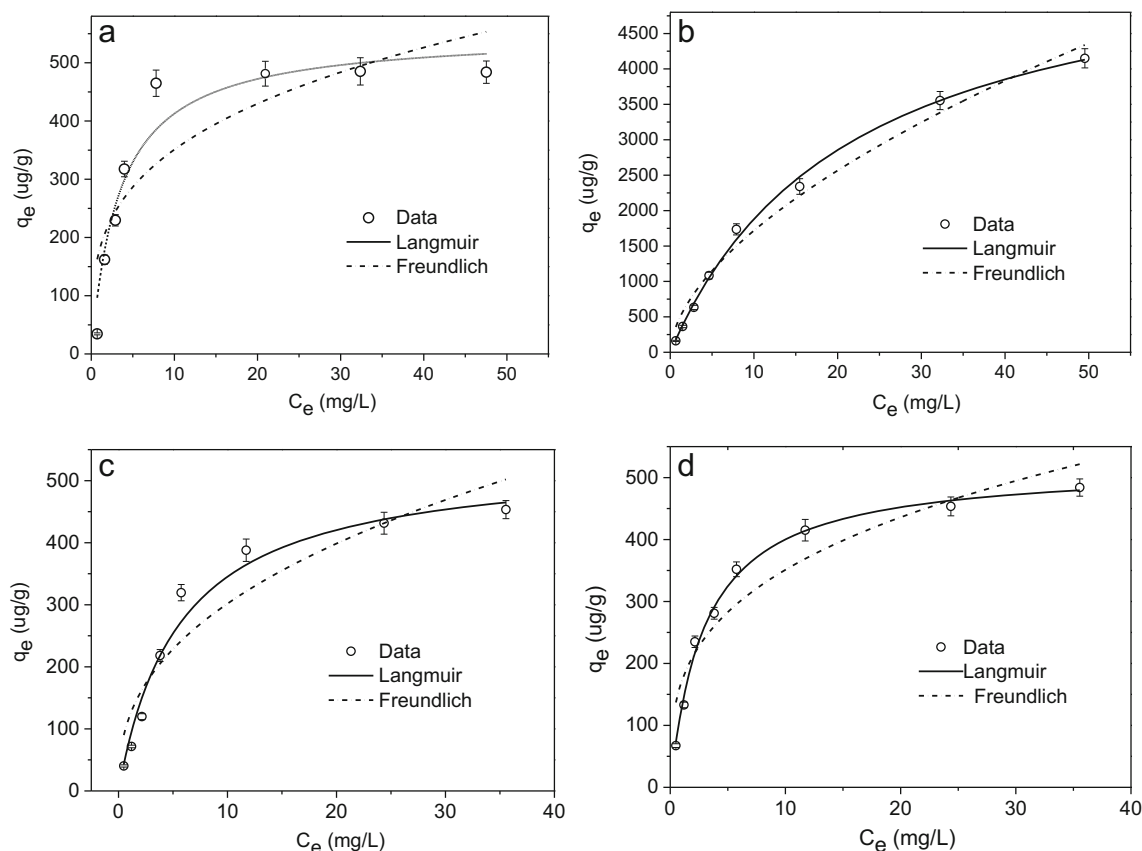
Fig. 5 Adsorption isotherm data and modeling for As onto adsorbents: **a** and **b** are As(V) adsorption on BC and RM-BC, respectively. **c** and **d** are As(III) adsorption on BC and RM-BC, respectively

adsorption elevated with the increasing of pH (Manju et al. 1998). Baig et al. (2014), using magnetic biochar, who noted that As(III) adsorption reached a maximum at pH = 8 (Baig et al. 2014). However, Yu et al. (2015) demonstrated that As(III) reached a maximum at pH = 3 with manganese oxide-modified biochar (Yu et al. 2015). This variation may be the result of the diverse adsorbents used in the investigations.

Adsorption kinetics

As(V) and As(III) kinetic experiments revealed that the sorption occurred rapidly firstly and then became slowly, finally reached equilibrium within 24 h (Fig. 4). First-order and second-order models were applied to elucidate mononuclear

and binuclear adsorption, while the Elovich model considered the influence of desorption. Compared with BC, RM-BC showed a greater sorption capacity for As. Table 1 listed kinetic models and best-fit parameter values for As adsorption data. Compared with other models, the data were much better conformed to the pseudo-second-order pattern for BC and RM-BC adsorbed As(V) (Table 1). However, for As(III) adsorption on BC and RM-BC, the fit is different. Between the four kinetic models, the former is more in favor of the pseudo-second-order model. When As(III) was adsorbed on RM-BC, the Elovich model agrees with the data more accurately.

The results showed that (1) the number of BC/RM-BC surface active sites probably impact the reaction rate in part and the rate- determining step will possibly due to chemical sorption in line with the pseudo-second-order kinetic model

Table 2 Isotherm models and best-fit parameters for As adsorption data

Sample		Langmuir			Freundlich		
		$k(\mu g^{-1})$	Q_{max} ($\mu g/g$)	R^2	$k(\mu g^{(1-n)} L^n g^{-1})$	n	R^2
BC	As(V)	0.296	552.0	0.949	179.2	0.293	0.786
RM-BC	As(V)	0.0465	5923.8	0.997	452.9	0.579	0.985
BC	As(III)	0.179	447.6	0.991	119.9	0.401	0.898
RM-BC	As(III)	0.333	520.0	0.995	171.2	0.312	0.911

Table 3 The maximum As(V) adsorption amount differed in various adsorbents

Adsorbents	Feedstock	q_{max} ($\mu g/g$)	References
Red mud modified biochar	Rice straw	5923.8	This work
Hematite modified biochar	Loblolly pine(*Pinus taeda*) wood	428.7	Wang et al. (2015a)
$MnCl_2 \cdot 4H_2O$ modified biochar	Pine wood	590	Wang et al. (2015b)
Birnessite modified biochar	Pine wood	910	Wang et al. (2015b)
Fe-coated biochars	Empty fruit bunch	15,200	Samsuri et al. (2013)
Fe-coated biochars	Rice husk	16,900	Samsuri et al. (2013)
La-loaded biochar	Corn stalk	38,020	Feng et al. (2015)
Red mud	–	941	Altundogan et al. (2000)

assumption. (Taty-Costodes et al. 2003; Mohan et al. 2011), (2) RM-BC adsorbed As(III) was a heterogeneous process and may be controlled by multiple mechanisms including chemisorption (Yao et al. 2014), and (3) both BC and RM-BC removed As(V) more effectively than As(III). Moreover, the adsorption amount of As(V) on RM-BC is more than that of BC.

Adsorption isotherms

Langmuir and Freundlich isotherms for As adsorbed onto BC and RM-BC are displayed in Fig. 5. With the increase of As concentration, As adsorption gradually rose until equilibrium was reached. In this study, all sorption isotherms were "L" shaped with higher R^2 compared with Freundlich (Table 2). The calculated Langmuir maximum adsorption capacity (Q_{max}) of RM-BC for As(V) and As(III) were 5923.8 and 520.0 $\mu g\ g^{-1}$ respectively. In contrast, the Q_{max} of BC for As(V) and As(III) were only 552.0 and 447.6 $\mu g\ g^{-1}$, respectively.

Langmuir isotherm is used to describe monolayer adsorption on sorbent surfaces. Both BC and RM-BC obey the adsorption mechanisms of Langmuir, which is in accordance

with many carbonaceous adsorbents (Zhang et al. 2013; Wang et al. 2015a). Red mud-modified biochar exhibited improved removal for As(V) and As(III) compared to BC, suggesting that it may enhance biochar adsorption sites (Wang et al. 2015a; Li et al. 2016).

In this work, R_L values for As(V) adsorption on BC and RM-BC and As(III) adsorption on BC and RM-BC were in the range of 0.0663–0.825, 0.303–0.970, 0.136–0.919, and 0.0778–0.860, respectively, indicating that adsorption was favorable.

Table 3 suggested that the maximum As(V) adsorption amount differed in various adsorbents. The Q_{max} of RM-BC for As(V) is inferior to the Q_{max} of Fe coated biochars (Samsuri et al. (2013)) and La loaded biochar (Feng et al. (2015)). Nevertheless, production of biochar treated with pure chemical reagents (Fe and La) would be expensive at an industrial level. Moreover, the Q_{max} of red mud modified biochar was much higher than that of other three biochar-based materials such as hematite modified biochar, $MnCl_2 \cdot 4H_2O$ modified biochar and birnessite modified biochar. Additionally, RM-BC is significantly better than pure red mud (Table 3).

Analysis of adsorption mechanisms

Considering RM-BC exhibited a better As(V) adsorption capacity than BC based on the above research results and As(III) is unstable that easy to be oxidized (Adra et al. 2015). Therefore, we investigate the mechanism of adsorption As(V) on RM-BC.

K-edge XANES analyses for As standards and RM-BC-As(V) are presented in Fig. 6. The excitation energies are displayed at 11872.4 and 11,876.5 eV corresponding to As(III) and As(V). It was revealed that both As species were adsorbed on the surface of the red mud by XANES spectra. Arsenate was the major species and accounted for 97.6% of the total As (Table 4). In addition, LCF results revealed three main As phases on RM-BC including hematite-As(V) (53.5%), magnetite-As(V) (33.8%), and gibbsite-As(V) (13.6%), which probably formed during the sorption process (Table 4).

Table 4 SPOIL values of references spectra of As(V) adsorption on RM-BC

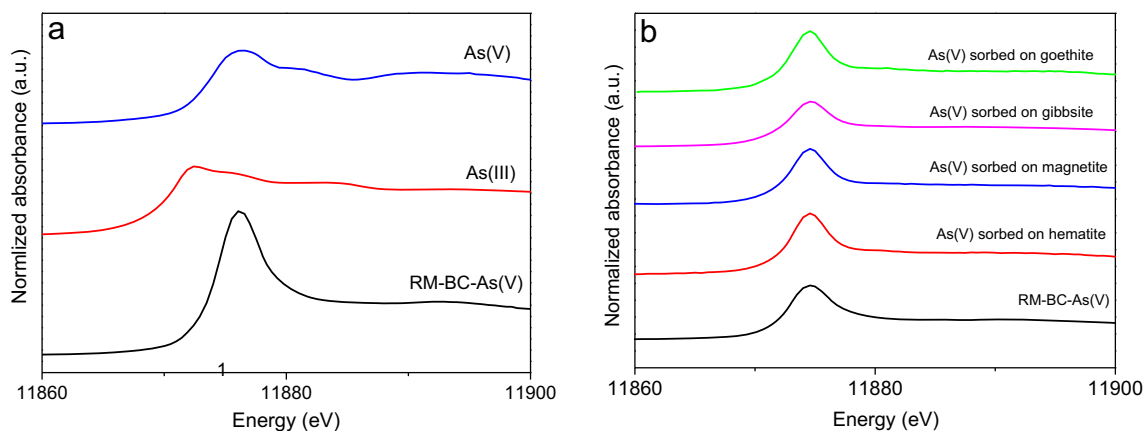| References	SPOIL Values		LCF results(%)
	Spoil	R	RM-As(V)
As(III)	0	0.01865	2.4
As(V)	0.3172	0.02239	97.6
R-factor			0.00868
Chi-square			0.0697
gibbsite-As(V)	0	9.16E-07	13.6
hematite-As(V)	0	1.37E-07	53.5
magnetite-As(V)	1.0423	5.61E-05	33.8
R-factor			0.00241
Chi-square			0.193

Fig. 6 Normalized As k-edge XANES spectra for As(V) adsorbed onto RM-BC **a** the percentages of As species; **b** the percentages of As adsorbed on different minerals

Previous studies demonstrated that the existence of iron and alumina oxides was indispensable to As sorption (Ding et al. 2017; Bai et al. 2016; Chen et al. 2017). It is revealed by XRD that hematite, goethite, magnetite, and gibbsite existed on RM-BC which is consistent with that reported in other studies which showed that the high temperature influence the components of red mud such as hematite and goethite (Liu and Naidu 2014). According to correlational research that high-temperature-treated hematite may lead some hematite turn to maghemite (Wang et al. 2015a). The diffraction peak of goethite has been reduced by reason of the chemical reaction $2FeOOH \rightarrow Fe_2O_3 + H_2O$. In other words, the mineral phrases transform from goethite to hematite gradually (Yang et al. 2015). The mechanism of gibbsite can be effectively bound to Arsenate mainly through forming inner sphere complexes (Ladeira et al. 2001). Hematite, magnetite, and goethite effectively reduced As

in aquatic environments, especially hematite demonstrating greatest adsorption capacity in acidic pH conditions (Gimenez et al. 2007; Mamindy-Pajany et al. 2011). Iron oxides can be able to effectively bound As mainly via ligands exchange forming inner sphere complexes (Mamindy-Pajany et al. 2011).

According to XANES results, possible adsorption mechanisms for As(V) on RM-BC are presented in Fig. 7. The structure M-O-As(V) formed may substantially enhanced the adsorption capacity of As(V). The possible mechanisms responsible for the adsorption of As on RM-BC may be similar to previous studies demonstrating that the mechanisms responsible for As adsorption on biochar are through electrostatic interactions, surface complexation (inner sphere surface monodentate and bidentate complexes), and chemical interactions between As and surface functional groups (Li et al. 2016; Zhang et al. 2013).

Fig. 7 Mechanism of As(V) adsorption on red mud-modified biochar, where M is the metal oxide composition of the red mud surface
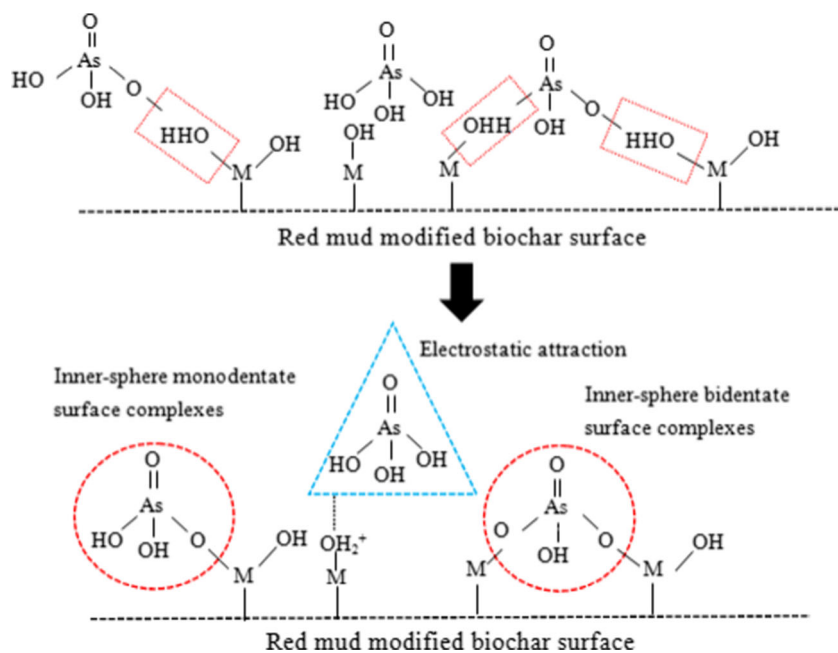
Conclusion

Red mud and rice straw biochar are promising materials for As-contaminated soil remediation due to their improved adsorbent capacity. A red mud-modified biochar (RM-BC) was created from red mud suspension treating biomass through pyrolysis. The kinetic processes of As(V) adsorption on RM-BC fitted the pseudo-second-order model, while that of As(III) favored the Elovich model. Moreover, all sorption isotherms produced improved fits for the Langmuir model. RM-BC revealed improved adsorption capacity of As(V) and As(III), with the maximum adsorption capacity ten times greater than that of the untreated biochar. XANES results indicated that the As(V) adsorbed onto RM-BC was possibly due to surface complexation and electrostatic interactions.

References

Adra A, Morin G, Nguema GO, Brest J (2015) Arsenate and arsenite adsorption onto Al-containing ferrihydrites implications for arsenic immobilization after neutralization of acid mine drainage. Appl Geochem 64:2–9

Altundogan HS, Altundogan S, Tumen F, Bildik M (2000) Arsenic removal from aqueous solutions by adsorption on red mud. Waste Manag 20:761–767

Bai YH, Yang TT, Liang JS, Qu JH (2016) The role of biogenic Fe-Mn oxides formed in situ for arsenic oxidation and adsorption in aquatic ecosystems. Water Res 98:119–127

Baig SA, Zhu J, Muhammad N, Sheng T, Xu X (2014) Effect of synthesis methods on magnetic Kans grass biochar for enhanced As(III, V) adsorption from aqueous solutions. Biomass Bioenergy 71:299–310

Castaldi P, Silvetti M, Enzo S, Melis P (2010) Study of sorption processes and FT-IR analysis of arsenate sorbed onto red muds (a bauxite ore processing waste). J Hazard Mater 175:172–178

Chen Z, Wang YP, Jiang XL, Fu D, Xia D, Wang HT, Dong GW, Li QB (2017) Dual roles of AQDS as electron shuttles for microbes and dissolved organic matter involved in arsenic and iron mobilization in the arsenic-rich sediment. Sci Total Environ 574:1684–1694

Cheng Q, Huang Q, Khan S, Liu Y, Liao Z, Li G, Ok YS (2016) Adsorption of cd by peanut husks and peanut husk biochar from aqueous solutions. Ecol Eng 87:240–245

Ding ZC, Fu FL, Cheng ZH, Lu JW, Tang B (2017) Novel mesoporous Fe-Al bimetal oxides for As(III) removal: performance and mechanism. Chemosphere 169:297–307

Feng Y, Xue L, Yang B, Liu Y, Duan J, He S, Yang L (2015) Adsorption of As from aqueous solution by lanthanum oxide-loaded biochar: process and mechanisms. J Agro-Environ Sci 34:2190–2197

Gimenez J, Martinez M, Depabio J, Rovira M, Duro L (2007) Arsenic sorption onto natural hematite, magnetite, and goethite. J Hazard Mater 141:575–580

Guo H, Guo HM, Yang LJ (2014) Simultaneous removal of fluoride and arsenic from aqueous solution using activated red mud. Sep Sci Technol 49:2412–2425

Hartley W, Riby P, Waterson J (2016) Effects of three different biochars on aggregate stability, organic carbon mobility and micronutrient bioavailability. J Environ Manag 181:770–778

Hua YM, Heal KV, Hanl WF (2017) The use of red mud as an immobiliser for metal/metalloid-contaminated soil: a review. J Hazard Mater 325:17–30

Jadhav SV, Bringas E, Yadav GD, Rathod VK, Ortiz I, Marathe KV (2015) Arsenic and fluoride contaminated groundwaters: a review of current technologies for contaminants removal. J Environ Manag 162:306–325

Khan S, Cai C, Waqa M, Arp HPH, Zhu YG (2013) Sewage sludge biochar influence upon rice (*Oryza sativa* L) yield, metal bioaccumulation and greenhouse gas emissions from acidic paddy soil. Environ Sci Technol 47:8624–8632

Kim EJ, Yoo J, Baek K (2014) Arsenic speciation and bioaccessibility in arsenic-contaminated soils: sequential extraction and mineralogical investigation. Environ Pollut 186:29–35

Kong XF, Guo Y, Xue SG, Hartley W, Wu C, Ye YZ, Cheng QY (2017a) Natural evolution of alkaline characteristics in bauxite residue. J Clean Prod 143:224–230

Kong XF, Li M, Xue SG, Hartley W, Chen CR, Wu C, Li XF, Li YW (2017b) Acid transformation of bauxite residue: conversion of its alkaline characteristics. J Hazard Mater 324:382–390

Ladeira ACQ, Ciminelli VST, Duarte HA, Alves MCM, Ramos AY (2001) Mechanism of anion retention from EXAFS and density functional calculations: arsenic (V) adsorbed on gibbsite. Geochim Cosmochim Acta 8:1211–1217

Li R, Wang JJ, Zhou B, Awasthi MK, Ali A, Zhang Z, Gaston LA, Lahori AH, Mahar A (2016) Enhancing phosphate adsorption by Mg/Al layered double hydroxide functionalized biochar with different Mg/Al ratios. Sci Total Environ 559:121–129

Liu Y, Naidu R (2014) Hidden values in bauxite residue (red mud): recovery of metals. Waste Manag 34:2662–2673

Lone AH, Najar GR, Ganie MA, Sofi JA, Ali T (2015) Biochar for sustainable soil health: a review of prospects and concerns. Pedosphere 25:639–653

Lu KP, Yang X, Gielen G, Bolan N, Okd YS, Niazi NK, Xu S, Yuan GD, Chen X, Zhang XK, Liu D, Song ZL, Liu XY, Wang HL (2017) Effect of bamboo and rice straw biochars on the mobility and redistribution of heavy metals (Cd, Cu, Pb and Zn) in contaminated soil. J Environ Manag 186:285–292

Mamindy-Pajany Y, Hurel C, Marmier N, Roméo M (2011) Arsenic (V) adsorption from aqueous solution onto goethite, hematite, magnetite and zero-valent iron: effects of pH, concentration and reversibility. Desalination 281:93–99

Manju GN, Raji C, Anirudhan TS (1998) Evaluation of coconut husk carbon for the removal of arsenic from water. Water Res 32:3062–3070

Mohan D, Rajput S, Singh VK, Steele PH, Pittman CU (2011) Modeling and evaluation of chromium remediation from water using low cost bio-char, a green adsorbent. J Hazard Mater 188:319–333

Samsuri AW, Sadegh-Zadeh F, Seh-Bardan BJ (2013) Adsorption of As(III) and As(V) by Fe coated biochars and biochars produced from empty fruit bunch and rice husk. J Environ Chem Eng 1:981–988

Sun L, Chen D, Wan S, Yu Z (2015) Performance, kinetics, and equilibrium of methylene blue adsorption on biochar derived from eucalyptus saw dust modified with citric, tartaric, and acetic acids. Bioresour Technol 198:300–308

Tan X, Liu Y, Gu Y, Xu Y, Zeng G, Hu X, Liu S, Wang X, Liu S, Li J (2016) Biochar-based nano-composites for the decontamination of wastewater: a review. Bioresour Technol 212:318–333

Taty-Costodes VC, Fauduet H, Porte C, Delacroix A (2003) Removal of Cd(II) and Pb(II) ions, from aqueous solutions by adsorption onto sawdust of *Pinus sylvestris*. J Hazard Mater 105:121–142

Wang SB, Ang HM, Tadé MO (2008) Novel applications of red mud as coagulant, adsorbent and catalyst for environmentally benign processes. Chemosphere 72:1621–1635

Wang S, Gao B, Zimmerman AR, Li Y, Ma L, Harris WG, Migliaccio KW (2015a) Removal of arsenic by magnetic biochar prepared from pinewood and natural hematite. Bioresour Technol 175:391–395

Wang S, Gao B, Li Y, Mosa A, Zimmerman AR, Mab LQ, Harris WG, Migliaccio KW (2015b) Manganese oxide-modified biochars: preparation, characterization, and sorption of arsenate and lead. Bioresour Technol 181:13–17

Wang T, Zhang LY, Wang HY, Li CF, Yang WC, Chai LY, Meng YD (2015c) Synthesis of core shell magnetic Fe_3O_4@poly(m-phenylenediamine) particles with high chromium removal performance. Environ Sci Technol 49:5654–5662

Wang N, Xue XM, Juhasz AL, Chang ZZ, Li HB (2017) Biochar increases arsenic release from an anaerobic paddy soil due to enhanced microbial reduction of iron and arsenic. Environ Pollut 220:514–522

Wu C, Zou Q, Xue SG, Pan WS, Yue X, Hartley W, Huang L, Mo JY (2016a) Effect of silicate on arsenic fractionation in soils and its accumulation in rice plants. Chemosphere 165:478–486

Wu C, Zou Q, Xue SG, Pan WS, Huang L, Hartley W, Mo JY, Wong MH (2016b) The effect of silicon on iron plaque formation and arsenic accumulation in rice genotypes with different radial oxygen loss (ROL). Environ Pollut 212(5):27–33

Wu C, Huang L, Xue SG, Pan WS, Zou Q, Hartley W, Wong MH (2017) Oxic and anoxic conditions affect arsenic (As) accumulation and arsenite transporter expression in rice. Chemosphere 165:478–486

Xia D, Tan F, Jiang CZ, Chen XZ, Li H, Zheng Y, Li Q, Wang Y (2016) $ZnCl_2$-activated biochar from biogas residue facilitates. Appl Surf Sci 377:361–369

Xue SG, Zhu F, Kong XF, Wu C, Huang L, Huang N, Hartley W (2016a) A review of the characterization and revegetation of bauxite residues (red mud). Environ Sci Pollut R 23(2):1120–1132

Xue SG, Kong XF, Zhu F, Hartley W, Huang N, Li XF (2016b) Proposal for management and alkalinity transformation of bauxite residue in China. Environ Sci Pollut R 23(11):12822–12834

Xue SG, Shi LZ, Wu C, Wu H, Qin YY, Pan WS, Hartley W, Cui MQ (2017) Cadmium, lead, and arsenic contamination in paddy soils of a mining area and their exposure effects on human HEPG2 and keratinocyte cell-lines. Environ Res 156:23–30

Yan XL, Lin LY, Liao XY, Zhang WB, Wen Y (2013) Arsenic stabilization by zero-valent iron, bauxite residue, and zeolite at a contaminated site planting Panax notoginseng. Chemosphere 93:661–667

Yao Y, Gao B, Fang J, Zhang M, Chen H, Zhou Y, Creamer AE, Sun Y, Yang L (2014) Characterization and environmental applications of clay-biochar composites. Chem Eng J 242:136–143

Yang F, Han T, Jin XZ, Wang HQ, Yang XT, Shen ZK (2015) Effect of thermal activation on mineralogical phases and activity of red mud. Fly Ash comprehensive utilization 2:3–5

Yu ZH, Huang Y, Lian F, Xie L, Liu S, Song Z (2015) Adsorption of arsenic(III) on biochar-manganese oxide composites. J Agro-Environ Sci 1:155–161

Zhang M, Gao B, Varnoosfaderani S, Hebard A, Yao Y, Inyang M (2013) Preparation and characterization of a novel magnetic biochar for arsenic removal. Bioresour Technol 130:457–462

Zhu F, Hou JT, Xue SG, Wu C, Wang QL, Hartley W (2017) Vermicompost and gypsum amendments improve aggregate formation in bauxite residue. Land Degrad Dev. doi:10.1002/ldr.2737

Zhu F, Liao JX, Xue SG, Hartley W, Zou Q, Wu H (2016a) Evaluation of aggregate microstructures following natural regeneration in bauxite residue as characterized by synchrotron-based X-ray micro-computed tomography. Sci Total Environ 573:155–163

Zhu F, Xue SG, Hartley W, Huang L, Wu C, Li XF (2016b) Novel predictors of soil genesis following natural weathering processes of bauxite residues. Environ Sci Pollut R 23(3):2856–2863

Zhu F, Zhou JY, Xue SG, Hartley W, Wu C, Guo Y (2016c) Aging of bauxite residue in association of regeneration: a comparison of methods to determine aggregate stability & erosion resistance. Ecol Eng 92:47–54